NJC

Accepted Manuscript

This is an *Accepted Manuscript*, which has been through the Royal Society of Chemistry peer review process and has been accepted for publication.

Accepted Manuscripts are published online shortly after acceptance, before technical editing, formatting and proof reading. Using this free service, authors can make their results available to the community, in citable form, before we publish the edited article. We will replace this *Accepted Manuscript* with the edited and formatted *Advance Article* as soon as it is available.

You can find more information about *Accepted Manuscripts* in the Information for Authors.

Please note that technical editing may introduce minor changes to the text and/or graphics, which may alter content. The journal's standard Terms & Conditions and the Ethical guidelines still apply. In no event shall the Royal Society of Chemistry be held responsible for any errors or omissions in this *Accepted Manuscript* or any consequences arising from the use of any information it contains.

ROYAL SOCIETY OF CHEMISTRY

www.rsc.org/njc

Journal Name

ARTICLE

Photoinduced Electron Transfer from Oxo-Mo^{IV}Selenolato Complex to Oxygen

Received 00th January 20xx,
Accepted 00th January 20xx

DOI: 10.1039/x0xx00000x

www.rsc.org/

Joyee Mitra[a†*] and Sabyasachi Sarkar[b*]

[NBu_4][MoO(mnt)(bpy)(SePh)].CH_2Cl_2 (**1**) and [NBu_4][MoO(mnt)(ophen)(SePh)].CH_2Cl_2 (**2**) complexes (mnt = maleonitriledithiolate ion; bpy = 2,2'-bipyridine, phen= 1,10-phenanthroline) stabilized by aromatic diimine have been synthesized and characterized. These complexes under aerobic condition on irradiation with sunlight (or with tungsten lamp) in solution generate superoxide radical concomitant to the formation of paramagnetic Mo(V) species due to a single electron transfer from the Mo(IV) complex to oxygen. The Mo(V) produced under photo-irradiation was characterized by EPR spectroscopy and the generated superoxide radical has been shown to transform nitrobluetetrazoleum (NBT) chloride to blue diformazan. Both **1** (and **2**) are phosphorescent having emission lifetime of 6-8 µs. Ground state and time dependent density functional theoretical calculation confirm that the electronic transitions from predominantly metal based molecular orbitals are responsible for the low-lying charge transfer excited states and also for the observed interaction with oxygen.

Introduction

Metallo-dithiolenes have gained importance due to their potential utility as Q-switch laser dyes, light conversion materials, in non-linear optics and as catalysts.[1] Transition metal complexes with aromatic diimine ligands like 2,2'-bipyridine, 1,10-phenanthroline and their derivatives are known to behave as photoactive energy or electron transfer agents depending on their ancillary ligands.[2] The ligand combination of diimine as the *pull ligand* and dithiolene as *push ligand* has been studied in square planar Ni, Pd and Pt complexes[3] but such combination with other metals having octahedral geometry was rare.

Many physiological processes involve stepwise electron transfer to activate dioxygen, producing free radical intermediates.[4] The limiting step in such oxidation processes is the first electron transfer forming superoxide radical. Synthetic models emulating such processes usually involve redox-active transition metal complexes for reductive activation of dioxygen to superoxo, peroxo or oxo species associated with an increase in the formal oxidation state of the metal. Monoxo molybdenum complexes are of some interest as they have been reported to exhibit photo-redox reactions.[5, 6]

In this article, we report the chemistry of two octahedral oxo-Mo^{IV}(diimine)(dithiolene)(selenolato) complexes bearing the *push-pull* ligand combination. The properties of the synthesized complexes are dominated by both ligands, one of which is easily oxidized and the other easily reduced.[3] We observed light induced electron transfer by these newly synthesized complexes, which have been studied by EPR, electrochemistry and by using density functional theoretical (DFT) and time dependent DFT calculations.[7]

Experimental

All reactions and manipulations were performed under argon using modified Schlenk technique. Solvents were dried and distilled according to standard procedures. [Na_2(mnt)][8] and [NBu_4]$_2$[Mo_2O_4(mnt)$_2$][9] were prepared following reported procedures.

Elemental analyses for carbon, hydrogen and nitrogen were carried out with Perkin-Elmer 2400 micro analyzer. FTIR spectra were recorded on a Bruker Vertex70 FT-IR spectrometer as pressed KBr pellets. Electronic spectra were recorded on Perkin-Elmer Lambda35 UV-visible spectrophotometer. Mass spectra (negative ion) were recorded on a Micromass QuattroI triple quadrupole mass spectrometer with an analytical electrospray source. The ESI capillary was set at 3.5 kV and the cone voltage was 20 V. Electron Paramagnetic Resonance spectra were recorded on Bruker Biospin EMX EPR X-Band Spectrometer with a frequency of 9.856 GHz. Samples for the chemically oxidized species of **1** (and **2**) were prepared using a previously reported method.[10] Small amount of I_2 (less than stoichiometric amount for one electron oxidation) was placed with **1** (and **2**) in the EPR tube under inert atmosphere. Few drops of dry, degassed

[a]*Department of Chemistry, Indian Institute of Technology Kanpur, Kanpur 208 016, Uttar Pradesh, India.*
[b]*Department of Chemistry, Indian Institute of Engineering Science & Technology Shibpur (IIEST), Howrah 711 103, West Bengal, India Email:abya@iitk.ac.in*
† Present address: DST – INSPIRE Faculty, DIMC, CSIR-CSMCRI Bhavnagar, Gijubhai Badheka Marg, Bhavnagar 364 002, Gujarat, India. Email: joyeemitra@csmcri.org
Electronic Supplementary Information (ESI) available: Details of X-ray crystallographic, spectroscopic data and DFT calculations are provided as supporting information. See DOI: 10.1039/x0xx00000x

DCM was allowed to move down the inner wall of the tube and as soon as the solid mixture of the complex and iodine was dissolved, the tube was cooled in liq. N_2 and placed in the pre-cooled Dewar attached to the EPR machine to record the spectra at 120 K. The sample was thawed in argon to record the room temperature EPR data. For experiments with oxygen, the thawed EPR sample was exposed to air briefly before refreezing. Spin quantitation was carried out using 1,3-bisdiphenylene-2-phenylallyl (BDPA) free radical as the standard. Cyclic voltammetric measurements of 10^{-3} M DCM solution of the compounds were recorded with glassy carbon electrode as working electrode with 0.2 M $[Bu_4N][PF_6]$ as supporting electrolyte, Ag/AgCl electrode as reference electrode, and platinum auxiliary electrode using BASi Epsilon, EC Bioanalytical Systems, Inc. All electrochemical experiments were carried out under argon at 298 K. Potentials are referenced against ferrocene/ferrocenium (Fc/Fc^+) and are reported relative to the Ag/AgCl electrode ($E_{1/2}(Fc^+/Fc)$) 0.459 V vs Ag/AgCl electrode).

X-Ray Crystallography: Diffraction-quality single crystals were glued to glass fibers and mounted on a BRUKER SMART APEX diffractometer equipped with CCD area detector. Data were collected using graphite-monochromated Mo K_α radiation (λ = 0.71069 Å) at low temperature (100 K). Cell constants were obtained from the least-squares refinement of three dimensional centroids through the use of CCD recording of narrow ω rotation frames, completing almost all-reciprocal space in the stated θ range. All data were collected with SMART 5.628 (BRUKER 2003), and were integrated with the BRUKER SAINT program.[11] Empirical absorption correction was applied using SADABS program. The structure was solved using SIR97 [12] and refined using SHELXL-97.[13] Crystal structures were viewed using ORTEP.[14] The respective space group of the compounds were determined on the basis of the lack of systematic absence and intensity statistics. Full-matrix least squares/difference Fourier cycles were performed which located the remaining non-hydrogen atoms. All non-hydrogen atoms were refined with anisotropic displacement parameters. Hydrogen atoms were added at idealized positions with uniform U_{iso} value. **2** possess one molecule in its asymmetric unit. In the asymmetric unit of **1**, there are two independent monomeric units of which one is structurally discussed with its ORTEP plot. Additional symmetry for **1** has been checked through PLATON, which did not suggest the presence of any additional symmetry in **1**. A c/2 pseudo-symmetry was found in **1**. Both **1** and **2** contain a DCM molecule in their crystal lattice.

Computational Details: Density-functional theory calculations were performed using the Gaussian 03 (Revision B.04) package.[15] Becke's three-parameter hybrid-exchange functional, the nonlocal correlation provided by the Lee, Yang, and Parr and Vosko, Wilk and Nuair 1980 local correlation functional (III) (B3LYP) [16] were employed. 6-31G*+ basis set was used for C, N, Se, S, O and H. For another set of calculations, BP86 [17] functional was used instead of B3LYP. The LANL2DZ basis set [18] and LANL2 pseudopotential of Hay and Wadt were used for Mo.[19] Klamt's conductor reaction field (COSMO) [20] solvent model was used for calculations with DCM solvent.

Synthesis: $[NBu_4][MoO(mnt)(bpy)(SePh)].CH_2Cl_2$ (**1**) 50 mg (0.05 mmol) of $[NBu_4]_2[Mo_2O_4(mnt)_2]$[9] was dissolved in 3 ml dichloromethane. 16 mg (0.1 mmol) of 2,2'-bipyridine was added into it followed by 6 fold excess of benzeneselenol and the mixture was stirred for 3 hrs. A greenish-blue solution was formed along with the precipitation of a red colored crystalline compound. The solution was filtered. To the filtrate petroleum ether (60°C-80°C) was added and it was allowed to stand undisturbed for two days at 4°C to obtain greenish-blue colored rectangular block shaped diffraction quality crystals. Yield 50% Analytical Data: $C_{37}H_{51}Cl_2MoN_5OS_2Se$, Mol.wt: 891.77, FTIR ($cm^{-1}$): ν_{CN} 2188, $\nu_{Mo=O}$ 924; Elemental analysis found (calculated) in % for $C_{37}H_{51}Cl_2MoN_5OS_2Se$; C 50.02 (49.83); H 5.93 (5.76); N 7.56 (7.85) m/z=612.37, anionic mass corresponding to $C_{20}H_{13}MoN_4O_4S_2Se^-$

$[NBu_4][MoO(mnt)(ophen)(SePh)].CH_2Cl_2$ (**2**) Similar procedure as in **1** was followed using 20.0 mg 1, 10-phenanthroline hydrate instead of bipyridine. Yield 55%. Analytical Data: $C_{39}H_{51}Cl_2MoN_5OS_2Se$, Mol. wt: 915.79, FTIR (cm^{-1}): ν_{CN} 2189, $\nu_{Mo=O}$ 927; Elemental analysis found (calculated) in % for $C_{39}H_{51}Cl_2MoN_5OS_2Se$; C 50.48 (51.15); H 5.73 (5.61); N 7.32 (7.65) m/z=636.40, anionic mass corresponding to $C_{22}H_{13}MoN_4O_4S_2Se^-$

Results and discussion

Structure description

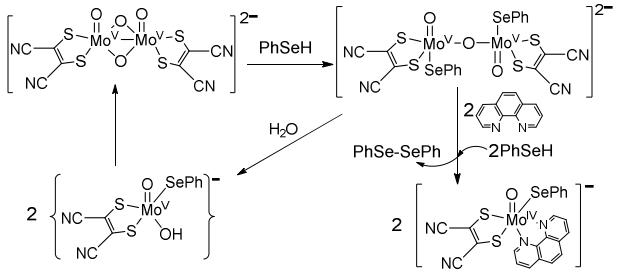

Scheme 1: Protonation of the $\{Mo^V_2O_4\}$ core and subsequent reduction and formation of **2** in the presence of PhSeH and 1,10-phenanthroline.

The $\{Mo^V_2O_4\}$ core in dioxo-bridged complexes can easily be protonated via the formation of intermediate monooxo-bridged species $\{Mo^V_2O_3\}$,[9] (Scheme 1) before complete cleavage of the bridged structure. This monooxo-bridged species is reverted back to the starting $\{Mo^V_2O_4\}$ core under favorable condition via a monomeric intermediate $\{OMo^V(OH)\}$ moiety.[9, 21] In the present synthesis selenol serves multiple roles: a proton source, a reducing agent and also as a coordinating ligand in the reaction with $\{Mo^V_2O_4\}$ core to yield monomeric oxo-Mo^{IV}(selenolato) species in the presence of aromatic diimines as chelating ligand. These selenolato complexes are synthesized faster compared to the iso-structural thiolato complexes,[10] owing to the rapid protonation of the $\{Mo^V_2O_4\}$ core by more acidic selenol (pK_a of

selenophenol is 4.6 and that of thiophenol is 6.0).[22] The monooxo-bridged dimeric Mo(V) intermediate once formed, responds to its reduction with excess of selenol yielding the stable monomeric Mo(IV) species coordinated to selenolato and to diimine as the co-ligand (Scheme 1). Such complexes are found to react with molecular oxygen under visible light illumination. The use of a robust chelating ligand like aromatic diimine is required to block the 5th and 6th coordination sites around molybdenum thereby negating the possibility of μ-oxo dimer formation, which is thermodynamically more stable compared to the monomeric pentavalent species.

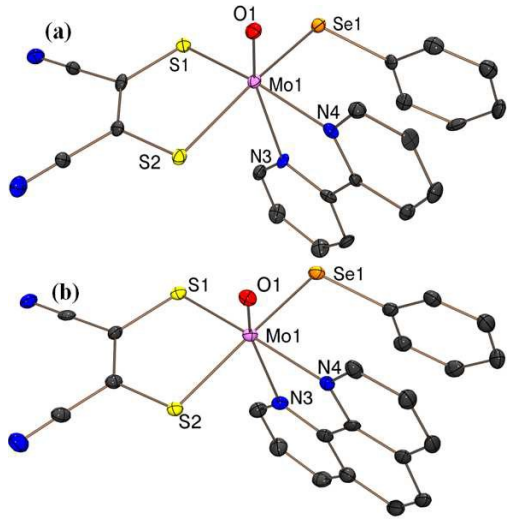

Figure 1: ORTEP plots of the crystal structures of the anions of (a) **1** and (b) **2** at 50% probability thermal ellipsoids with partial atom labeling scheme.

Figure 1(a) and (b) show the crystal structures of the anions of $1{\bullet}CH_2Cl_2$ and $2{\bullet}CH_2Cl_2$ respectively. The molybdenum center is coordinated to a terminal oxo, two sulfur atoms from the dithiolene ligand, two nitrogen atoms from the diimine and a selenolato moiety in each case. As expected the Mo atom is raised above the basal plane comprising two sulfur, one selenium and one nitrogen atom by ~0.34 Å for both **1** and **2** adopting a distorted octahedral structure. The Mo-Se bond distance of 2.558(1) Å is slightly longer compared to other reported hexacoordinated complexes [23] indicating a single bond character between Mo and Se atoms. The Mo=O distance of 1.693(4) Å is similar to other reported Mo^{IV}-oxo species.[10, 23] The two diimine nitrogen atoms are coordinated to the molybdenum center at a distance of 2.231(3) and 2.310(5) Å respectively. The Mo-N bond *trans* to oxo is longer by ~0.08 Å due to the strong trans effect of the molybdenyl group. O=Mo-N4 and O=Mo-N3 angles are 86.2(2)° (86.1(2)°) and 155.8(2)° (156.4(2)°) respectively for **1** (and **2**). Observed O=Mo-Se angles is 101.62 (15)° and 102.66(14)° for **1** and **2** respectively. C-S distances of 1.746(6) and 1.737(7) Å and average C=C bond distance of 1.383(9) Å are in good agreement with reported values.[23] Diimine bite 70.00(18)° (70.55(18)° for **2**) and dithiolene bite 84.37(6)° and (84.24(5)°) are observed for **1** (and **2**) respectively. The pertinent bond distances and angles are provided in ESI-Table S2.

Spectroscopic Behavior

A low energy solvatochromic band appeared around 600 nm and another more intense band around 390 nm for both **1** and **2** (Figure 2). A substantial shift to longer wavelength (24-28 nm) is observed in acetone compared to DCM indicating the charge transfer character of the electronic transition (Figure S1, ESI). It is known that due to a transient charge separation in the excited state, metal complexes with diimine ligands exhibit a light induced charge transfer transition.[24]

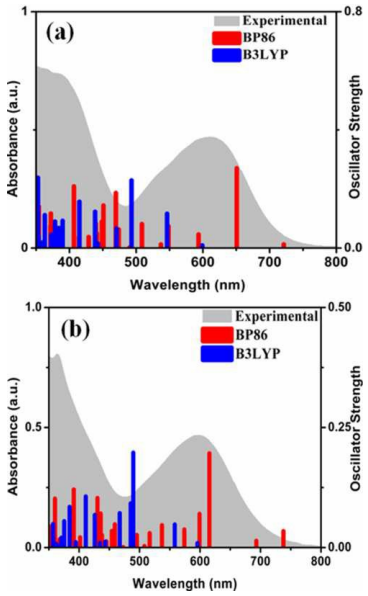

Figure 2: Electronic spectra of 10^{-4}M solutions of (a) **1** and (b) **2** in DCM (grey shade) and the TDDFT calculated electronic transitions. Red and blue bars are related to the use of BP86 and B3LYP functional respectively in DCM as the solvent.

TDDFT calculations were carried out to identify the main features of the absorption spectra.[3, 25] Both B3LYP and BP86 functional were employed in calculations incorporating DCM as solvent. The electronic spectra are characterized by a high density of states between 350 nm – 500 nm assigned mainly to intra-ligand transitions involving $n \rightarrow \pi^*$ and $\pi \rightarrow \pi^*$ transitions of both diimine and dithiolene. The excited states between 550-700 nm have considerable metal contribution and can be assigned as MLCT transitions (HOMO → LUMO (LUMO+1) (ESI-FigS2-S3, Table S3-S4). Time dependent density functional theoretical calculation (TDDFT) supports the involvement of metal d-orbital in the transition to diimine excited state. Such an assignment is common in M(diimine)(dithiolene) complexes.[3, 25] Our experimental data are more in agreement with BP86 functional derived results for the MLCT transitions. Calculated MLCT with B3LYP function are at much lower wavelength compared to experimental data. Similar observations of failure of B3LYP functional have been reported elsewhere.[26] Deviations from the experimental results are often reported for TDDFT, as the calculations are

dependent on basis sets, exchange – correlation functional, solvent models etc.[27] The MLCT state resulted in chemical change that may be best explained by considering an intermediate resembling an anion radical (oxidized metal and reduced ligand).[28]

Photo-physical properties of {MoO} depend on their oxidation state; pentavalent complexes are fluorescent (life time ~110 ns for $OMoCl_4(CH_3CN)^-$)[5] while tetravalent complexes sometimes show phosphorescence. [6]

On excitation of degassed DCM solutions of **1** (and **2**) at 390 nm, a strong emission is observed around ~470 nm with a less intense peak ~650 nm. The oxo-Mo^{IV} complexes are known to be phosphorescent in solution having a life time of ~2.5 µs (±10%) for $[MoOCl(CN\text{-}^tBu)_4][BPh_4]$.[6] The enhancement of the lifetime (6.21 µs and 8.72 µs for **1** and **2** respectively) in comparison to literature value may be due to the presence of chromophoric diimine in these complexes. The lifetime values are consistent with emission from triplet state. The singlet excited states of **1** (and **2**) are populated on photoexcitation, followed by a fast inter-system crossing (ISC) resulting in the formation of MLCT excited state with a dominant triplet character. This state is responsible for the observed phosphorescence. Close lying π - π * and MLCT states along with the presence of a heavy metal results in an increased spin – orbit coupling and thus the efficiency of radiative deactivation pathway increases.[29] Quenching of emission is observed in the presence of dioxygen similar to other phosphorescent complexes. These results are supported by TDDFT calculations (ESI Table S5).

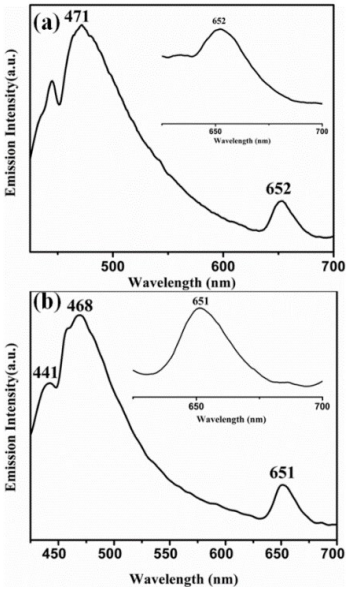

Figure 3: Phosphorescent emission spectra of (a) **1** and (b) **2** in DCM (λ_{ex}, 390 nm). Inset shows the emission ~650 nm.

EPR Analysis

EPR silent Mo(IV) complexes **1** (and **2**) were chemically oxidized by one electron under inert atmosphere at room temperature (and at 120K) to record X-band EPR spectrum. Characteristic Mo(V) EPR spectrum was observed with six hyperfine lines and g = 1.992 (Figure 4(a)). EPR spectrum of **1** (and **2**) in DCM at 120K is axial with g =2.028 and $g_\perp$=1.992 (Figure 4b). High g value of **1** (and **2**) can be attributed to the Mo-Se coordination, resulting in enhanced delocalization of the unpaired electron over selenium p-orbitals. Hyperfine interaction of Mo based unpaired electron with Se nucleus is considerably smaller than the line width of the spectrum, thus no splitting is observed due to ^{77}Se (I = ½, 7.63% natural abundance, possessing low magnetic moment 0.53506, and its contribution to electron density in SOMO is very small (Fig. 7)) in the EPR spectrum. The spectrum does not exhibit super-hyperfine coupling to N (I=1) center in support of the absence of unpaired electron density on the diimine ligands in HOMO (SOMO). Spin quantitation of the Mo(V) signal using BDPA radical as the integration standard gave 0.75±0.05 spins per molecule for both **1** and **2** (i.e. approximately 1 spin per monomeric molybdenum species).

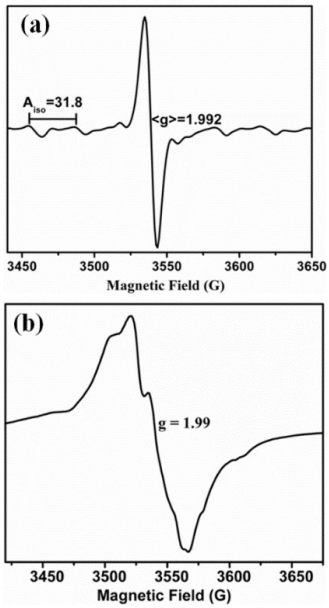

Figure 4: X-band EPR spectra of chemically oxidized **1** in DCM solution (a) at room temperature and (b) at 120K.

Interestingly, a similar EPR signal was observed on irradiating a solution of **1** (and **2**) in air using a 100 W tungsten lamp (Figure 5a). Around 20 min. of irradiation resulted in the appearance of an EPR signal with g=1.992 from the initial EPR silent solution. However, this signal was found to disappear on prolonged exposure to light. Suitable color filters were employed to identify the wavelength range most suitable for photo-excitation. Such filters accompanied with cooling of the light exposed solution took care of the heat generated by the tungsten lamp. We observed that the complexes responded sluggishly with 0.1M $K_2Cr_2O_7$ solution (yellow-orange filter) to generate EPR signal compared to 0.1 M $CuSO_4$ solution (blue) or 0.1 M $CoCl_2$ solution (pink-red) filter. EPR spectrum observed in all three cases consisted of one intense g=1.992 signal at room temperature. **1** (or **2**) has strong absorbance in

the visible region. Consequently, their photo-induced electron transfer could be initiated by selective excitation with low energy visible light. Irradiation of deoxygenated solutions of **1** (or **2**) do not show any EPR activity supporting the involvement of dissolved oxygen in generating the observed Mo(V) EPR signal. Also, solution of **1** (or **2**) on standing in the dark did not show any EPR signal when exposed to air. It should be mentioned that the isostructural thiolato complexes [10] do not show any photo-activation under similar conditions.

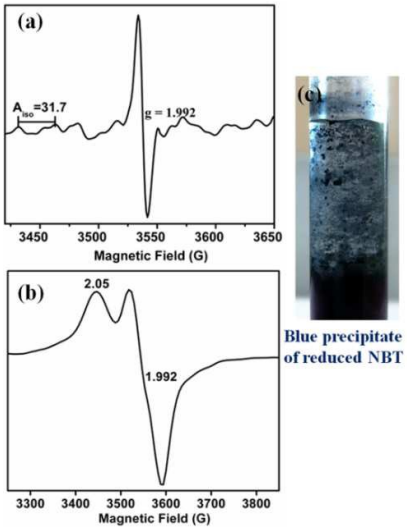

Figure 5: X-band EPR spectrum of **1** in solution under light irradiation in air (a) at room temperature and (b) at 120K. (c) Blue precipitate of diformazan from reduced NBT confirming superoxide formation with a solution of **1** in air and on exposure to sunlight.

On flash freezing the solution of **1** (or **2**) after light irradiation, a broad anisotropic EPR signal was observed which consisted of two components g =2.05 and g⊥=1.992 (Figure 5b). These could be merged signals of Mo(V) species and superoxide radical. The presence of superoxide radical has been identified previously in frozen solutions from the characteristic EPR signal having g 2.08 (broad line) and g⊥ 2.00, detected during oxidation by molecular oxygen.[30, 31] On warming this solution to room temperature, only a symmetric six-line signal characteristic of Mo(V) was observed. The MLCT excited state generated on excitation of the singlet ground state of **1** (and **2**) followed by a fast ISC can be quenched by molecular O_2 via electron transfer to generate $O_2^{\cdot-}$.Superoxide anion radical is known to be temperature sensitive.[30] Due to rapid rotation in solution, an extremely broad signal for $O_2^{\cdot-}$ is expected which is inversely related to its spin relaxation time and thus, precludes its detection by EPR spectroscopy at room temperature. Detection is possible only in frozen solutions where the orbital degeneracy is lifted.[32] Quantification of the superoxide radical was difficult as it is known to react with Mo(V) converting it to Mo(VI)[33] and also with DCM in a multistep process consuming one or more of the radical species per chloride to yield oxygenated products albeit at a sluggish rate. [34]

The generation of superoxide radical ($O_2^{\cdot-}$) upon photo-induced single electron transfer from **1** (and **2**) in air has been confirmed chemically using nitrobluetetrazolium (NBT) test.[35] Reduction of the pale yellow NBT dye to blue colored diformazan was used to detect the presence of superoxide[36] (Figure 5c). The diformazan was extracted into aqueous phosphate buffer and quantified using a known concentration of $[Me_4N][O_2]$ [37] to record an average of ~60% conversion. No change in color from yellow NBT to blue diformazan was observed under inert atmosphere. Thus, **1** and **2** generate superoxide radical ion upon irradiation with visible light concomitant with the oxidation of the complexes to Mo(V) where dioxygen acts as the external oxidant. A scheme for the photo-induced reaction of **1** (and **2**) with oxygen has been presented in scheme 2.

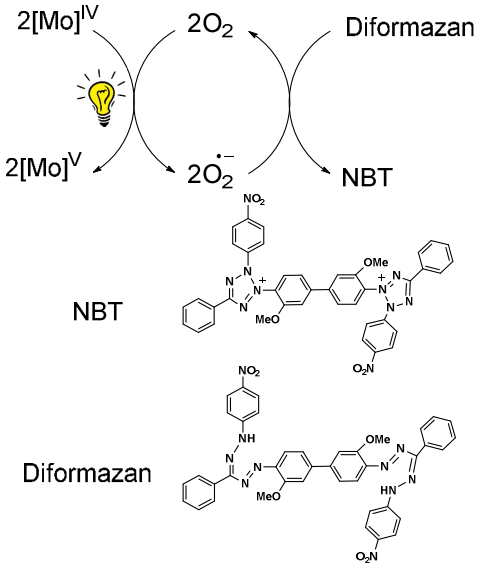

Scheme2: Reaction scheme for the generation of superoxide on photoexcitation of Mo(IV) species in **1** concomitant to its oxidation to Mo(V). Superoxide radical further reacts with NBT forming diformazan.

Electrochemistry

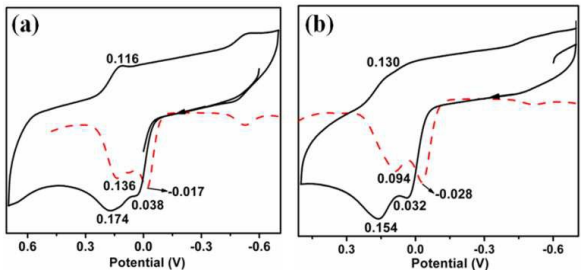

Figure 6: Cyclic voltammograms of (a) **1** and (b) **2** in DCM at a scan rate of 100mV/s. Differential pulse polarogram are shown as dashed traces.

The change of the equatorial ligand from thiolate to selenolate has a marked effect on the redox potential in these complexes.[10] One electron oxidation of both **1** and **2** occur at -0.017 V for **1** and -0.028 V for **2** respectively (vs Ag/AgCl), (Figure 6). The one electron oxidized species loses another electron almost simultaneously following successive two steps of one electron oxidation processes. Both the oxidation waves

are due to the loss of an electron from the molybdenum centre for **1** (and **2**). This has been supplemented by the observation of Mo d_{xy} based HOMO (and SOMO) for the complexes and their one electron oxidized species (*vide* computational analysis). Two oxidative processes become clearer on increasing the scan rate to 0.5V/s (ESI- Figure S4 and S5). Both these oxidations are quasi-reversible, supporting the very short lifetime of the intermediate oxidized species. A peak at -0.6V appears on repeated scanning and is not characteristic of **1** and **2**. It may appear due to species adsorbed on the electrode surface or may be due to some follow-up electrochemical reactions.

Computational Analysis

Geometry optimization reproduced the structural features from the crystallographic analysis of **1** and **2**. Average deviation of 0.02 – 0.03 Å in the bond lengths were observed. Such a small difference between crystallographic and optimized geometries are not unusual and may originate from crystal packing effects.

A predominantly Mo d_{xy} based HOMO and a HOMO - 1 delocalized on S and Se p orbitals are obtained. The LUMO and LUMO +1 are delocalized over diimine ligand, supporting MLCT transition as the origin of the low energy band in the electronic spectra. On one electron oxidation of the complexes, the HOMO retains its metal character (Figure 7). A decrease in HOMO - LUMO gap is observed for both **1** and **2** with BP86 calculations compared to B3LYP due to destabilization of HOMO and stabilization of LUMO. The HOMO-LUMO gap decreases in Mo(V) species as compared to the corresponding Mo(IV) species in both the functional. This is more prominent in the calculations with BP86. HOMO of Mo(IV) and Mo(V) species are energetically similar for both the complexes as calculated using BP86 functional (calculated orbitals energies for Mo(IV) and Mo(V) are -90.86 kcalmol^{-1} and -86.01 kcalmol^{-1} respectively) as compared with the results from B3LYP functional (calculated orbitals energies for Mo(IV) and Mo(V) are -109.99 kcalmol^{-1} and -88.87 kcalmol^{-1} respectively) (Figure 7, ESI Table S6). Thus, results from BP86 functional are consistent to the experimentally observed closely spaced electrochemical responses.

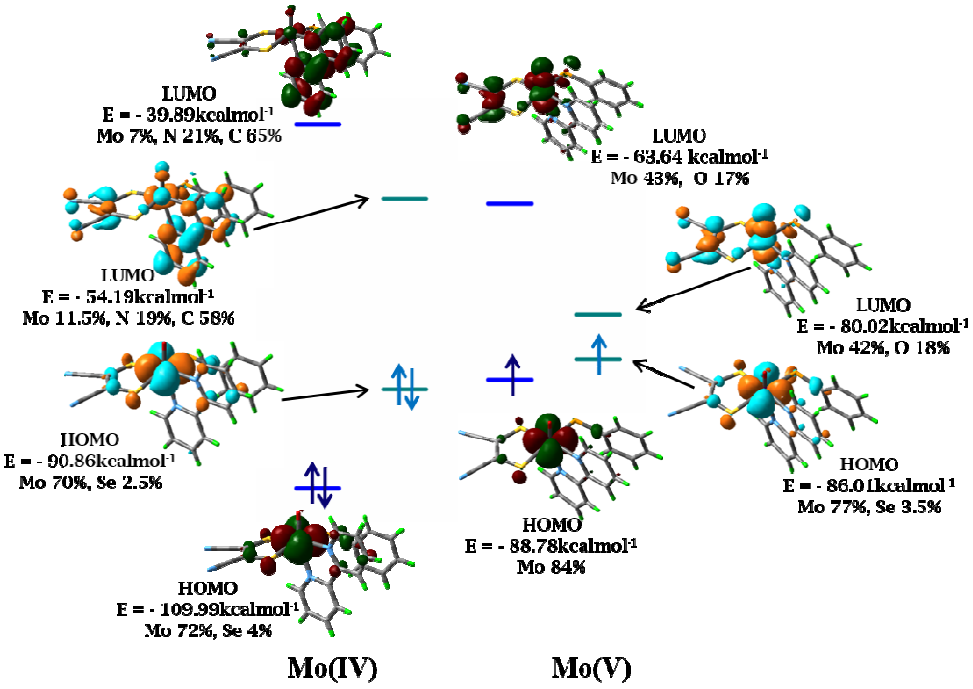

Figure 7: Frontier orbital images of **1** and its one electron oxidized species in DCM using B3LYP (red and green) and BP86 (orange and cyan) functional respectively. Iso-surface cutoff value 0.04. The energy levels corresponding to B3LYP and BP86 have been depicted in blue and cyan respectively.

Charge analysis on metal and surrounding ligand atoms revealed a positive charge on Mo which increases slightly upon one electron oxidation, consistent with the removal of an electron from the metal center. According to Mulliken spin population analysis, the unpaired electron is localized on the Mo center, consistent with the oxidation of Mo(IV) (d^2 system) to Mo(V) (d^1 system). The percentage of metal d orbital in HOMO is of great importance as the nature of the frontier orbitals and electronic transitions are helpful in analyzing the photo-activity and electrochemistry of the complexes. Thus, an appropriate choice of diimine and dithiolene would allow predetermination of the nature of lowest energy transitions and the emitting states.

It is known that a change in geometry of the species concerned can alter the population of molecular orbital. To address this aspect, a single point energy calculation has also

been performed with the one electron oxidized species without geometry optimization, which essentially yields almost the same population of molecular orbitals thereby eliminating the possibility of severe alteration of population in the molecular orbitals due to a change in the geometry.

Conclusions

Oxo-Mo^{IV}(diimine)(dithiolene)(selenolato) complexes participate in facile photo-induced single electron transfer to dioxygen producing superoxide radical concomitant to the generation of EPR active Mo(V) species. Generation of superoxide has been supported from the classical biochemical NBT test. Significantly increased lifetime were recorded for both the phosphorescent complexes compared to previously reported oxo-Mo^{IV} species, attributed to the presence of aromatic diimine ligands. Time dependent density functional theoretical calculations were employed conjointly with ground state calculations to support the experimentally observed photo-activation of the synthesized complexes and to rationalize the observed metal based single electron transfer.

Acknowledgements

SS acknowledges DST, India for funding. JM thanks DST-INSPIRE Faculty award.

Notes and references

‡ Crystallographic data for **1**: Empirical formula $C_{37}H_{51}Cl_2MoN_5OS_2Se$, Formula wt: 891.77 Crystal system Triclinic, Space group P -1, a 9.562(5) Å b 19.281(5) Å c 23.109(5) Å, α 79.293(5)° β 83.660(5)° γ 77.619(5)°, V 4077.88 $Å^3$, Z 4. Crystallographic data for **2**: Empirical formula $C_{39}H_{51}Cl_2MoN_5OS_2Se$, Formula wt: 915.79 Crystal system Triclinic, Space group P -1, a 9.288(5) Å b 11.771(5) Å c 19.492(5) Å α 83.300(5)° β 84.385(5)° γ 83.738(5)° V 2096.03, Z 2. **CCDC 826727** and **CCDC 826728** contain the crystallographic data for **1** and **2**. These can be obtained free of charge from the Cambridge Crystallographic data Centre via www.ccdc.cam.ac.uk/data_request/cif

1 V. P. Mueller-Westerhoff and D. I. Yoon, *Tetrahedron*, 1991, **47**, 440; M. Hissler, J. E. McGarrah, W. B. Connick, D. K. Geiger, S. D. Cummings and R. Eisenberg, *Coord. Chem. Rev.*2000, **208**, 115; N. Robertson and L. Cronin, *Coord Chem Rev* 2002, **227**, 93.
2 G. A. Crosby, *Acc. Chem. Res.* 1975, **8**, 231; L. Spiccia, G. B. Deacon and C. M. Kepert, *Coord. Chem. Rev*. 2004, **248**, 1329; J. H. Alstrum-Acevedo, M. K. Brennaman and T. J. Meyer, *Inorg. Chem*. 2005, **44**, 6802; F. G. Gao and A. J. Bard, *J. Am. Chem. Soc.* 2000, **122**, 7426.
3 C. A. Mitsopoulou, *Coord. Chem. Rev*. 2010, **254**, 1448; S. D. Cummings, R. Eisenberg, *Inorg. Chem*. 1995, **34**, 2007.
4 D. T. Sawyer, in *Oxygen Chemistry*; Oxford University: New York, 1991.
5 J. R. Winkler and H. B. Gray, *Comments Inorg. Chem.* 1981, **1**, 257; A. K. Mohammed and A. W. Maverick, *Inorg. Chem.* 1992, **31**, 4441.
6 R. A. Isotovich, A. S. Beadle, F. R. Fronczek and A. W. Maverick, *Inorg. Chem.* 1998**,** **37**, 4258.
7 C. Jamorski, M.E. Casida and D.R. Salahub, *J. Chem. Phys.* 1996, **104,** 5134.
8 E. I. Stiefel, L. E. Bennet, Z. Dori, T. H. Crawford, C. Simo and H. B. Gray, *Inorg. Chem.* 1970, **9**, 281.
9 K. Pal, R. Maiti, P. K. Chaudhury and S. Sarkar *Inorg. Chim. Acta,* 2007, **360**, 2721.
10 J. Mitra and S. Sarkar, *Inorg. Chem*. 2013, **52**, 3032.
11 SAINT, version 5.6; Bruker AXS Inc.: Madison, WI, 2000
12 A. Altomare, M. C. Burla, M. Camalli, G. L. Cascarano, C. Giacovazzo, A. Guagliardi, A. G. G. Moliterni, G. Polidori and R. Spagna, *J. Appl. Crystallogr.* 1999, **32**, 115.
13 G. M. Sheldrick, SHELX97. Programs for Crystal Structure Analysis (Release 97-2); University of Göttingen: Göttingen, Germany, 1997.
14 L. J. Farrugia, *J. Appl. Crystallogr*. 1997, **30**, 565.
15 Gaussian 03, Revision B.04, M. J. Frisch, G. W. Trucks, H. B. Schlegel, G. E. Scuseria, M. A. Robb, J. R. Cheeseman, J. A. Montgomery, Jr., T. Vreven, K. N. Kudin, J. C. Burant, J. M. Millam, S. S. Iyengar, J. Tomasi, V. Barone, B. Mennucci, M. Cossi, G. Scalmani, N. Rega, G. A. Petersson, H. Nakatsuji, M. Hada, M. Ehara, K. Toyota, R. Fukuda, J. Hasegawa, M. Ishida, T. Nakajima, Y. Honda, O. Kitao, H. Nakai, M. Klene, X. Li, J. E. Knox, H. P. Hratchian, J. B. Cross, V. Bakken, C. Adamo, J. Jaramillo, R. Gomperts, R. E. Stratmann, O. Yazyev, A. J. Austin, R. Cammi, C. Pomelli, J. W. Ochterski, P. Y. Ayala, K. Morokuma, G. A. Voth, P. Salvador, J. J. Dannenberg, G. A. Zakrzewski, S. Dapprich, A. D. Daniels, M. C. Strain, O. Farkas, D. K. Malick, A. D. Rabuck, K. Raghavachari, J. B. Foresman, J. V. Ortiz, Q. Cui, A. G. Baboul, S. Clifford, J. Cioslowski, B. B. Stefanov, G. Liu, A. Liashenko, P. Piskorz, I. Komaromi, R. L. Martin, D. J. Fox, T. Keith, M. A. Al-Laham, C. Y. Peng, A. Nanayakkara, M. Challacombe, P. M. W. Gill, B. Johnson, W. Chen, M. W. Wong, C. Gonzalez, and J. A. Pople, Gaussian, Inc., Wallingford CT, 2004.
16 A. D. Becke, *J. Chem. Phys.* 1993, **98**, 5648; C. Lee, W. Yang and R. G. Parr, *Phys. Rev. B.* 1988, **37**, 785.
17 A. D. Becke, *Phys. Rev. A,* 1988, **38**, 3098; J. P. Perdew, *Phys. Rev. B*, 1986, **33**, 8822.
18 G. A. Patersson and M. A. Al-Laham, *J. Chem. Phys.* 1991, **94**, 6081.
19 P. J. Hay and W. R. Wadt, *J. Chem. Phys.* 1985, **82**, 270; W. R. Wadt and P. J. Hay, *J. Chem. Phys*. 1985, **82**, 284.
20 F. Eckert and A. Klamt, *AIChE J.* 2002, **48**, 369.
21 J. Mitra and S. Sarkar, *Ind. J. Chem. Sect A,* 2011, **50A**, 401.
22 J. Huang, C. Li, S. P. Nolan and J. L. Petersen, *Organometallics* 1998, **17**, 3516.
23 H. Tano, R. Tajima, H. Miyake, S. Itoh and H. Sugimoto, *Inorg. Chem.* 2008, **47**, 7465; B.S. Lim, R. H. Holm *J. Am. Chem. Soc* 2001, **123**, 1920; A Majumdar and S. Sarkar *Coord. Chem. Rev*. 2011, **255**, 1039; R. H. Holm, E. I. Solomon, A. Majumdar and A. Tenderholt *Coord. Chem. Rev*. 2011, **255**, 993.
24 J**.** K. Nagle, J. S. Bernstein, R. C. Young and T. J. Meyer, *Inorg. Chem***.** 1981**, 20,** 1760; K. Kalyanasundaram, *Coord. Chem. Rev.,* 1982**, 46,** 159
25 A. Vl˘cek Jr. and S. Záliš, *Coord. Chem. Rev.* 2007, **251**, 258; M. Buhl, C. Reimann, D. A. Pantazis, T. Bredow and F Neese, *J. Chem. Theory Comput.* 2008, **4**, 1449
26 B. Champagne, M. Guillaume, F. Zutterman, Chem. Phys. Lett. 2006, 425, 105; N. A. Besley and F. A. Asmuruf, Phys. Chem. Chem. Phys., 2010, 12, 12024
27 C. Adamo and D. Jacquemin, Chem. Soc. Rev. 2013, 42, 845; A. D. Laurent and D. Jacquemin, Int. J. Quant. Chem. 2013, 113, 2019
28 P. P. Zarnegar and D**.** G. Whitten, ***J.*** *Am. Chem,*. Soc., 1971, **93**, 3776; P. P. Zarnegar, C. R. Bock and D. G. Whitten, *J. Am. Chem. Soc*. 1973, **95**, 4367.
29 F. D. Angelis, S. Fantacci, N. Evans, C. S. M. Klein, C. Zakeeruddin, J.-E. Moser, K. Kalyanasundaram, H. J. Bolink, M. Gratzel and M. Nazeeruddin, *Inorg. Chem*. 2007**, 46**, 5989.
30 R. N. Bagchi, A. M. Bond, F. Scholz and R. Stosser, *J. Am. Chem. Soc*. 1989, **111**, 8270

31 P. F. Knowles, J. F. Gibson, F. M. Pick and R. C. Bray, *Biochem J.* 1969, **111**, 53
32 D. T. Sawyer, G. Chiercato, Ch. T. Angelis, E. J. Nanni and T. Tsuchiya *Anal. Chem*. 1982, **54**, 1720
33 Y. Sasaki, *Bull Chem Soc Jpn* 1977, **50**, 1939.
34 J. L. Roberts, Jr. and D. T. Sawyer *J. Am. Chem. Soc*. 1981, **103**, 712
35 B. H. J. Bielski, G. G. Shiue and S. Bajuk, *J. Phys. Chem.* 1980, **84**, 830; J. E. Ryer- Powder and H. Forman, *J. Free Radic. Biol. Med.* 1989, **6**, 513.
36 K. V. Rajagopalan and P. Handler, *J. Biol. Chem.* 1964, **239**, 2022; R. W. Miller, *Can. J. Biochem*. 1970, **48**, 935; C. O. Beauchamp and I. Fridovich, *Anal. Biochem* 1971, **44,** 276.
37 D. Bhattacharya, S. Maji, K. Pal and S. Sarkar *Inorg. Chem*. 2008, **47**, 5036.

Table of Contents (TOC) entry

Photoinduced Electron Transfer from Oxo-Mo^{IV}Selenolato Complex to Oxygen

Joyee Mitra[a†*] and Sabyasachi Sarkar[b*]

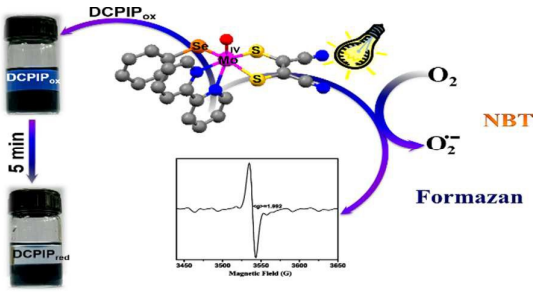

Electron transfer from oxo-Mo^{IV}(selenolato) complex under visible light generates superoxide radical concomitant to the oxidation of Mo^{IV} to Mo^{V}.